Int J Fract (2010) 162:21–31
DOI 10.1007/s10704-010-9481-x

ORIGINAL PAPER

Crack propagation in brittle heterogeneous solids: Material disorder and crack dynamics

Laurent Ponson · Daniel Bonamy

Received: 11 July 2009 / Accepted: 13 March 2010 / Published online: 7 April 2010

Abstract Crack propagation in a linear elastic material with weakly inhomogeneous failure properties is analyzed. An equation of motion for the crack is derived in the limit of slow velocity. Predictions of this equation on both the average crack growth velocity and its fluctuations are compared with recent experimental results performed on brittle heterogeneous materials (Ponson in Phys Rev Lett, 103, 055501; Måløy et al. in Phys Rev Lett, 96, 045501). They are found to reproduce quantitatively the main features of crack propagation in disordered systems. This theoretical framework provides new tools to predict life time and fracture energy of materials from their properties at the micro-scale.

Keywords Inhomogeneous materials · Growth velocity of cracks · Velocity fluctuations

1 Introduction

Integrating the effect of material micro-structure and heterogeneities into a theoretical framework describing their failure is a very challenging task. Because of the divergence of the stress field at the tip of a crack, material breakdown is crucially determined by a small region close to this tip. This leads to fundamental difficulties in homogenizing and averaging local properties to obtain the overall failure response of heterogeneous materials. As a result, there is no consistent theory that relates toughness fluctuations at the micro-scale with macroscopic failure properties, as fracture energy or lifetime.

Here, we focus on brittle materials with weakly heterogeneous local properties in the quasi-static limit. Following the approach pioneered by Gao and Rice (1989) and later extended by Schmittbuhl et al. (1995), and Ramanathan et al. (1997), we rigorously extend the "standard" Linear Elastic Fracture Mechanics (LEFM) developed for homogeneous materials to the case of heterogeneous media by considering a random field of fracture energy. In this type of models, the motion of a crack is analogous to the one of an elastic line driven in a random medium and critical failure occurs when the external force is sufficiently large to depin the crack front from the heterogeneities of the material. This approach succeeded to account for the effective toughness distribution in brittle disordered materials (Charles et al. 2004) or the large scale morphological scaling features of post-mortem fracture surfaces (Bonamy et al. 2006; Ponson 2007). Here, we address the problem of the dynamics of a crack propagating in a 3D material analyzing in detail the relation between the external loading conditions and the crack driving force. After deriving the equation of motion of a crack

L. Ponson (✉)
Graduate Aerospace Laboratories (GALCIT), California Institute of Technology, Pasadena, CA 91125, USA
e-mail: ponson@caltech.edu; laurent.r.ponson@wanadoo.fr

D. Bonamy
CEA, IRAMIS, SPCSI, Group Complex Systems and Fracture, 91191 Gif sur Yvette, France

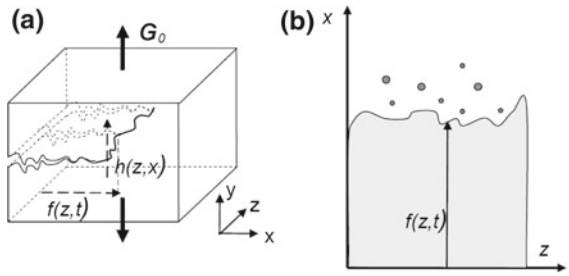

Fig. 1 Sketch and notations of a crack front propagating in a 3D heterogeneous material (**a**). To first order, the equation of motion involves the in-plane component $f(z,t)$ of the crack front and can be reduced to the one of a planar crack front propagating within a 2D material (**b**)

(Sec. 2), the predictions of the model are compared in Sec. 3 with recent experimental results on the dynamics of cracks propagating in heterogeneous brittle solids (Ponson 2009; Måløy et al. 2006). We show that the main features of *both* average dynamics and its fluctuations can be reproduced quantitatively by the proposed stochastic extension of Fracture Mechanics to inhomogeneous media. Implications of this theoretical framework on the roughness properties of cracks are then briefly described, and its relevance for predicting fracture energy and life time of materials from their properties at the micro-scale is finally discussed.

2 Equation of motion for a crack in an inhomogeneous medium

In this section, we derive the equation of motion for a crack propagating within a linear elastic inhomogeneous material. The scheme presented in Fig. 1a provides a description of the considered system as well as the notations used in the following. Because of the material heterogeneities, the crack front does not correspond to a straight line, and is described by its in-plane $f(z,t)$ and out-of-plane deviations $h(x,z)$. As a result, a point of the crack front is defined by its coordinates $(f(z,t), h(f,z), z)$. Locally, the crack front wants to take advantage of the area with low fracture energy to propagate at a lower energy cost within the material. On the other hand, large front distortions are expensive in term of mechanical energy and are then limited by the system "elasticity". This is the balance between these two effects that will be analyzed in the following.

To understand this competition more quantitatively, let us consider a given point on the crack front, and derive the expressions of the local energy release rate—driving force for the crack motion—and the local fracture energy. Expressed both with respect to crack deviations from straightness, they will both serve as a basis for the derivation of the equation of motion for the crack, that provides the local velocity all along the front.

The local—space dependent—fracture energy is described by the following stochastic field:

$$G_c(x,y,z) = \Gamma_0 + \delta\Gamma\eta(x,y,z), \tag{1}$$

where the random term $\eta(x,y,z)$ is chosen to be correlated over a length ξ and to have zero mean and unity variance. This simply means that the fracture energy in two points of the specimen separated by a distance larger than ξ—a typical heterogeneity length-scale—are uncorrelated. On a general manner, the function η, related to microscopic properties of the material, is not known. However, as we will discuss later, the macroscopic failure properties of heterogeneous materials will depend only on the mean value of the fracture energy $\Gamma_0 = \langle G_c(x,y,z)\rangle_{x,y,z}$ (where the operator $\langle\rangle_{x,y,z}$ means averaging over space) and its fluctuations through the second moment of the fracture energy distribution $\delta\Gamma = (\langle G_c(x,y,z)^2\rangle_{x,y,z} - \Gamma_0^2)^{1/2}$.

Material inhomogeneity generates distortions on the crack trajectory. Those, in turn, generate variations of the elastic energy release rate $G(z,t)$ along the front. For small perturbations, the variations of $G(z,t)$ depend on the in-plane distortions $f(z,t)$ only (Ball and Larralde 1995; Movchan et al. 1998), so that the 3D problems we are considering here reduces to the 2D problem represented in Fig. 1b. In this equivalent problem, the crack propagates within the mean fracture plane with a fracture energy $G_c(x = f(z,t), y = h(x = f(z,t), z), z)$ that reduces to $G_c(x = f(z,t), z)$ because h is determined independently.[1] In other words, for slightly heterogeneous brittle materials, out-of-plane deviations, and therefore fracture surface roughness-, have no effect on the crack dynamics as well as on the effective fracture energy of the solid. The variations of the elastic energy released have been derived by Rice (1985). Assuming that $\frac{\partial f}{\partial z} \ll 1$, to first order, one gets:

[1] The out-of-plane crack deviations h, corresponding to the fracture surfaces left behind after full propagation, can be described by an equation decoupled from the equation of motion based on the principle of local symmetry (see Ramanathan et al. 1997; Bonamy et al. 2006; Ponson 2007).

$$G(z,t) = G_0(f(z,t),t) + \frac{G_0\overline{f}(z,t)}{\pi} \times \int \frac{f(z',t)-f(z,t)}{(z'-z)^2}dz' \quad (2)$$

where the integral is defined in the principal value (pv) sense (see e.g. Bower and Ortiz 1991 for a detailed discussion of the discretization procedure). The quantity G_0 is the energy release rate corresponding to a straight crack of length $\overline{f}(t) = \langle f(z,t)\rangle_z$ (where the operator $\langle\rangle_z$ means averaging over z co-ordinate only). We make here the choice to express the average macroscopic energy release rate $G_0(\overline{f}(t),t)$ imposed to the specimen with respect to the crack length and the time. The effect of the time dependence of the force or displacement effectively applied to the solid during the fracture test is therefore implicitly implemented into the temporal variations of G_0.

Finally, one can derive the equation of motion for the crack by relating its local velocity $\frac{\partial f(z,t)}{\partial t}$ to the local elastic energy released $G(z,t)$ and the local fracture energy $G_c(x = f(z,t), z)$. This is possible by considering the kinetic energy of the solid associated with an elementary crack extension, as done in Freund (1990). The relation obtained locally at point $(x = f(z,t), z)$ is:

$$G_c(x = f(z,t), z) = \left(1 - \frac{1}{v_r}\frac{\partial f(z,t)}{\partial t}\right) G(z,t), \quad (3)$$

which can be further simplified by considering the limit of small crack velocities with respect to the Rayleigh wave speed v_r. This leads to:

$$\frac{1}{v_r}\frac{\partial f(z,t)}{\partial t} \simeq \frac{G(z,t) - G_c(x = f(z,t), z)}{G_c(x = f(z,t), z)} \quad (4)$$

This equation can be recast using Eq. (1). To first order in $\delta\Gamma/\Gamma_0$, one gets:

$$\frac{1}{\mu}\frac{\partial f(z,t)}{\partial t} \simeq G(z,t) - \Gamma_0 - \delta\Gamma\eta(f(z,t),z), \quad (5)$$

with $\mu = \frac{v_r}{\Gamma_0}$. Reporting Eq. (2) in the previous expression leads to

$$\frac{1}{\mu}\frac{\partial f(z,t)}{\partial t} = G_0(f(z,t),t) - \Gamma_0 + \frac{G_0(\overline{f}(t),t)}{\pi} \times \int \frac{f(z',t)-f(z,t)}{(z'-z)^2}dz' - \delta\Gamma\eta(f(z,t),z) \quad (6)$$

This gives the general form of the motion equation for a crack in an infinite material with sufficiently weak heterogeneities so that Rice's formula (Eq. 2), derived for a slightly perturbed crack, remains valid (see Adda-Bedia et al. (2006), for the effect of larger perturbations).[2]

To go further in the analysis of this equation of motion, we will consider the motion of the crack when its length is larger than, but close to, a length c_0. The reference $t = 0$ is taken as the time scale for which $G_0(c_0, t = 0) = \Gamma_0$. As a result, the variations of the external loading can be approximated by

$$G_0(f(t),t) - \Gamma_0 \simeq -k[(f(t) - c_0) - v_m t] \quad (7)$$

where $k = -\frac{\partial G_0}{\partial \overline{f}}\|_{\overline{f}=c_0,t=0}$ and $v_m = -\frac{\frac{\partial G_0}{\partial t}\|_{\overline{f}=c_0,t=0}}{\frac{\partial G_0}{\partial \overline{f}}\|_{\overline{f}=c_0,t=0}}$. For a stable geometry corresponding to $k > 0$, note that v_m corresponds to the stationary velocity reached by the crack on the time span considered, while the compliance k is a "spring constant" of a restoring force that maintains the position of the crack close to its equilibrium position $v_m t$ imposed by the external loading. As a result, the crack is driven by an effective quadratic potential that moves at the velocity v_m.[3] Keeping only first order terms in f and t, one finally gets

$$\frac{1}{\mu}\frac{\partial f(z,t)}{\partial t} = -k[(f(z,t) - c_0) - v_m t] + \frac{G_0(c_0,0)}{\pi}\int \frac{f(z,t)-f(z',t)}{(z-z')^2}dz' - \delta\Gamma\eta(f(z,t),z) \quad (8)$$

In the following, we will limit our analysis to a stable geometry ($k > 0$). Under this condition, Eq. (8) describes the motion of the crack front as the one of an elastic line driven in a random potential by a quadratic potential moving at the velocity v_m. As a result, after a short transient regime, the crack velocity is also v_m and imposed by the external loading conditions, as far as the development made in Eq. (7) is a good approximation of the variations of $G_0(\overline{f}(t),t)$.[4]

Equations similar to the equation of motion of a crack (Eq. 8) are involved in many physical situations where elastic systems are embedded in a material containing random impurities, such as vortex lines,

[2] Our approach based on the first order formula of Eq. (2) remains valid as far as the slope $\partial f/\partial z$ is small with respect to 1. In particular, there is no need that f is small with respect to a characteristic dimension of the geometry.

[3] The equilibrium position of the crack front satisfies the condition $G_0(\overline{f},t) = \Gamma_0$, and c_0 is chosen as the equilibrium position at t=0. It is worth to note that the average crack length is always slightly shorter than $v_m t$ for a stable geometry.

[4] This condition defines an acceptable range of timescale $t < t^*$.

domain walls or charge density waves. As a result, this equation has been largely studied, both from a numerical point of view (Rosso and Krauth 2002; Duemmer and Krauth 2007), or using an approximated analytical approach based on renormalization group theory (Ertas and Kardar 1994; Chauve et al. 2001). Note however that these studies did not considered the effect of the quadratic potential that drives the crack motion ($k = 0$), but used a constant external driving force. This effect was studied in Rosso et al. (2007), and Bonamy et al. (2008), and the crack front was shown to display quantitatively similar behaviors in both situations.

At first, it is important to separate two different situations: for crack perturbations $|\delta f(z,t)| = |f(z,t) - \overline{f}(t)| \ll \xi$ where ξ corresponds to the typical size of material heterogeneities, the stochastic term reduces to $\eta(\overline{f}, t)$.[5] In that case, the equation of motion is linear in f and can be solved by Fourier transform as e.g. in Pindra et al. (2008). However, for more disordered media, the crack deformations are too large to allow for such an approximation, and the non-linearity due to the stochastic term results in a rich and complex dynamics of the crack such as pinning of the front at small external loading and a stick slip motion close to the depinning threshold. In the following, we will focus on this regime, corresponding to the experimental situation investigated in Sec. 3.

The mechanism of crack pinning by the material heterogeneities is described in Fig. 2 where the average crack velocity $\langle \overline{v} \rangle = \langle \frac{\partial f}{\partial t} \rangle_{z,t}$ (where the operator $\langle \rangle_{z,t}$ means averaging over both z-co-ordinate and time) is represented as a function of the elastic restoring rate $G_0(\overline{f}(t), t)$ applied to the solid. At zero temperature, crack propagation is prohibited for small driving force $G_0 < \Gamma_0 + \Delta G_c$, so that the effective fracture energy of the heterogeneous solid is:

$$G_c^{\text{eff}} = \Gamma_0 + \Delta G_c, \tag{9}$$

i.e. the average of the local values of fracture energy in the solid plus a positive constant ΔG_c. This additional constant results from the pinning of the front by the material disorder η and will be discussed further in the discussion section of this manuscript. Above the pinning threshold, the mean velocity $\langle v \rangle$ of the crack front

[5] For perturbations $|\delta f(z,t)| \ll \xi$, the stochastic term can be written as $\eta(f(z,t),z) = \eta(\overline{f}(z,t) + \delta f(z,t), t) \simeq \eta(\overline{f}(z,t),t) + \delta f(z,t) \frac{\partial \eta(\overline{f}(z,t),t)}{\partial z}$ where the second term is of second order, and negligible with respect to the other terms of Eq. (8).

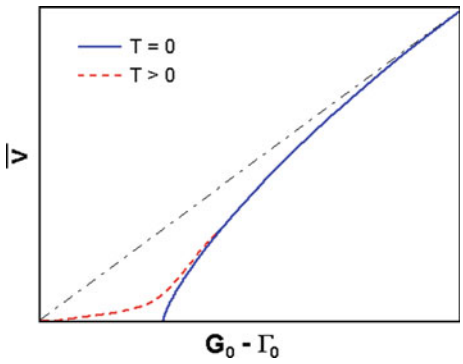

Fig. 2 Sketch showing the variations of the average crack velocity $\langle \overline{v} \rangle = \langle \frac{\partial f(z,t)}{\partial t} \rangle_{z,t}$ with the elastic energy release rate G_0. The *dash straight line* corresponds to the situation of an homogeneous material with $\delta\Gamma = 0$ and hence, $\langle v \rangle / \mu = G_0 - \Gamma_0$. The *plain line* corresponds to the situation of an inhommogeneous brittle solid ($\delta\Gamma > 0$) at zero temperature ($T = 0$) where the crack motion is described by Eq. (8). The *dashed line* shows the effects of a finite temperature ($T > 0$) so that thermally activated processes enable subcritical motion

scales as $(G_0 - G_c^{\text{eff}})^\theta$ where θ is called the velocity exponent. Equation (8) studied using functional renormalization group techniques (Ertas and Kardar 1994; Chauve et al. 2001) provides $\theta = 0.78$ and $\theta = 0.59$ to first and second order in perturbation, respectively. Recent direct numerical simulations results in $\theta \simeq 0.63$ (Duemmer and Krauth 2007). Note that such properties of the solution of Eq. (8) are independent of the stochastic term η. This enables to derive predictions on the macroscopic behavior of the crack in a brittle solid, even if the field of fracture energy is not known at the micro-structure scale.

3 Confrontation with experimental results

3.1 Average dynamic of a crack

In this section, we investigate the variations of the average crack velocity with the elastic energy release rate G_0 for an inhomogeneous material, and compare it with the theoretical predictions of Sec. 2. Sandstone is chosen as an archetype of heterogeneous elastic materials. A Botucatu sandstone, made of quartz grains with a diameter $d = 230\ \mu\text{m} \pm 30\ \mu\text{m}$ and a porosity $\phi = 17 \pm 2\ \%$, is used for the experiments.

We use an original experimental setup to measure the variations of crack velocity from slow to very fast propagation in brittle materials. Contrary to the

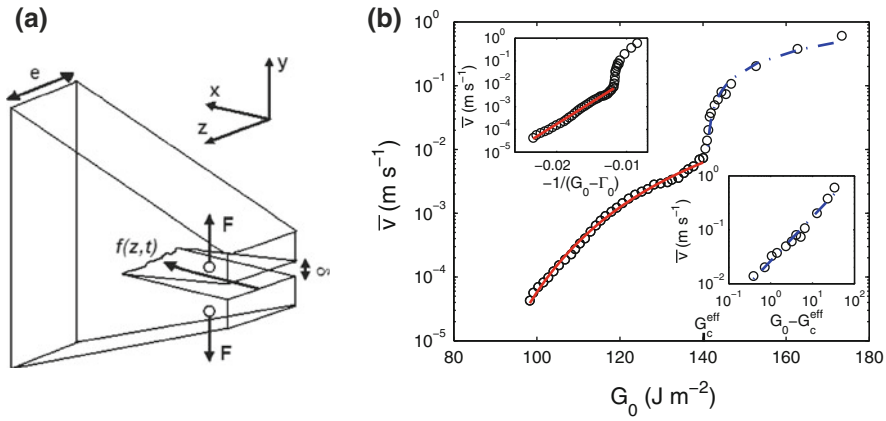

Fig. 3 Effect of material heterogeneities on the average dynamic of a crack: **a** Sketch of the fracture test; **b** variations of the average crack velocity with its driving force G_0 as measured experimentally for a brittle inhomogeneous rock. Both subcritical (*solid line*) and critical (*dashed line*) regimes are captured by the model of failure of disordered media

torsion tests classically used to measure the $\overline{v}(G_0)$ curves in rocks (Atkinson 1984; Nara and Kaneko 2005), the Tapered Double Cantilever Beam specimens used in the experiments (Fig. 3a) result in a slight and controlled acceleration of the crack produced by the tapered shape of the samples. As a consequence, it is possible to measure crack velocities up to $\simeq 1$ m s^{-1} not achieved by classical fracture tests. In addition, the external tensile loading produces relatively straight crack fronts, allowing a simple interpretation of the experiments. Finally, a straight crack propagation is obtained without lateral guide grooves that produce a large scattering of the experimental $\overline{v}(G_0)$ curves (Nara and Kaneko 2005).

An initial notch $c_0 = 35$ mm is machined in 100 mm long samples with thickness $e = 30$ mm. They are submitted to a uniaxial traction by increasing the displacement $\delta_F = v_{ext}t$ at the velocity $0.2\ \mu$m s$^{-1} \leq v_{ext} \leq 4\ \mu$m s^{-1} between two rods previously inserted in the drilled specimens. During the test, a force gauge measures the applied tension F while a clip gage measures the opening displacement δ between the two lips of the crack with a precision of 100 nm. From the measured values of δ and F, one obtains the variations of the specimen compliance $\lambda^{exp}(t) = \delta(t)/F(t)$ that can be used to measure the average position of the crack front $\overline{c}(t) = \langle c(z,t)\rangle_z$ while it propagates. The method is based on Finite Element (FE) simulations of an elastic specimen in the same geometry: We run several simulations with various values of the crack length $\overline{c}$ to obtain the variations of the compliance $\lambda^{FE}(\overline{c}) = \delta/F$ as a function of the crack length. This function is then compared with the experimental value of the compliance $\lambda^{exp}(t)$ in order to measure the crack length $\overline{c}(t)$ at each time step t. From the evolution of the crack length, it is now possible to measure the crack speed $\overline{v} = \frac{d\overline{c}}{dt}$ as well as the driving force G_0 imposed to the system during the test (see Ponson 2009 for more details).

The variations of the crack velocity with the driving force as observed on the sandstone specimens are represented in Fig. 3b in semi-logarithmic coordinates. Velocity measurements are achieved over almost five orders of magnitude, corresponding to a relatively small variation of the driving force. Irrespective of the external loading rate v_{ext}, the failure behavior of the rock is found to be characterized by two very different regimes defining G_c^{eff}. Near, but above this critical loading, a slight change in the driving force results in a strong variation in the crack velocity. This high sensitivity is studied in more detail in the bottom right inset of Fig. 3b, where $\overline{v}$ is plotted as a function of the net driving force $G_0 - G_c^{eff}$ in logarithmic coordinates. The linear behavior in this representation suggests a power law variation of the crack velocity

$$\overline{v} \sim (G_0 - G_c^{eff})^{\theta} \quad \text{for } G_c^{eff} < G_0 \tag{10}$$

with $G_c^{eff} = 140 \pm 3$ J m^{-2} and $\theta = 0.80 \pm 0.15$.

According to the theoretical predictions of Sec. 2, this power law behavior suggests that a *depinning transition* from a pinned to a moving crack as described in Eq. (8) occurs at $G_0 = G_c^{eff}$. Note that such interpretation of the failure of inhomogeneous materials had already been suggested by experiments made on other kinds of materials for which damage processes play a crucial role, preventing a quantitative comparison with the predictions of Linear Elastic Fracture Mechanics (Daguier et al. 1997).

The variations of velocity at driving forces $G_0 < G_c^{eff}$ are now studied. According to the model proposed in Sec. 2 at zero temperature, the external driving force is too low, and the crack front is pinned

by the material heterogeneities. However, at room temperature T, thermally activated processes can enable a subcritical propagation. The kinetics of the crack in this regime, described by adding an annealed noise $\eta_T(z,t)$ to Eq. (8), is provided by an Arrhenius law $\overline{v} \sim e^{-\frac{E_a}{k_B T}}$ where E_a is the activation energy for bond rupture and k_B is the Boltzmann constant. This subcritical propagation gives rise to a collective motion of the line characteristic of glassy systems, with a typical energy barrier $E_a \sim (G_0 - \Gamma_0)^{-\mu}$ where $\mu = \frac{2\zeta_{eq}}{1-\zeta_{eq}} \simeq 0.60$ for long-range elasticity (Feigelman et al. 1989; Kolton et al. 2005) for which $\zeta_{eq} \simeq 0.23$ is the roughness exponent characterizing the line perturbations at thermal equilibrium (Le Doussal et al. 2004). As a result, the crack velocity is given by

$$\overline{v} \sim e^{-\frac{C}{k_B T (G_0 - \Gamma_0)^{\mu}}} \quad \text{for } G_0 < G_c^{\text{eff}}. \tag{11}$$

This so-called creep law, first proposed for the subcritical crack dynamics in Ponson et al. (2007) and then observed in the context of paper peeling (Koivisto et al. 2007), describes rather well the experimental measurements presented here over the whole range of subcritical loadings $G_0 < G_c^{\text{eff}}$.

Contrary to the critical regime, slow crack propagation in rocks has been largely investigated and shown to depend crucially on the temperature (Atkinson 1984; Nara and Kaneko 2005). Analytical forms such as $\overline{v} \sim e^{\frac{-E^*}{k_B T}} G_0^{n/2}$ (Charles 1959) or $\overline{v} \sim e^{-\frac{E_0 - bG_0}{k_B T}}$ (Wiederhorn et al. 1974) were proposed. Both formulas reproduce correctly the measurements reported here, but on a smaller range of values of external crack driving force $G_0 < 120\ \text{J.m}^{-2}$. The first one, largely used because of its rather simple and compact form characterized by one subcritical crack growth index, leads to $n \simeq 34$ that compares well with the other experimental findings for sandstone (Atkinson 1984). The second formula leads to $b \simeq 0.68 \times 10^{-20}\ \text{m}^2$ which is also in agreement with the other measurements made on rocks with a similar microstructure (Nara and Kaneko 2005). This last description is based on the Arrhenius law $\overline{v} \sim e^{-\frac{E_a}{k_B T}}$ where the activation energy $E_a = E_0 - b\,G_0$ represents the typical barrier along the energy landscape tilted by the external force G_0. Indeed, large values of G_0 corresponding to high tensile forces increase the probability of bond rupture by thermal activated processes, such as e.g. thermal stress fluctuations (Santucci et al. 2004) and chemical reactions (Wiederhorn 1967). However, this theoretical approach supposes that the typical energy barrier remains independent of the geometry of the crack front. This assumption is perfectly fair as far as one considers the motion of a crack tip in a 2D medium, but in the more realistic situation of a 3D inhomogeneous material, the crack line can take advantage of the material elasticity to deform and explore an energy landscape rather different from the raw fluctuations produced by the material heterogeneities. The creep law with activation energy $E_a \sim (G_0 - \Gamma_0)^{-\mu}$ captures such a mechanism.

3.2 Fluctuations of crack velocity

We turn now to the predictions of the LEFM stochastic description of crack growth in terms of velocity fluctuations and compare it to experimental observations performed by Måløy et al. (2006) on the slow crack propagation along a weak heterogeneous plane within a transparent PMMA block according to the geometry depicted in Fig. 4a. In this specific geometry, the relation between G_0 and the mean crack length $\overline{f}$ can be obtained using beam theory (Obreimoff 1930), and the parameters k and v_m in Eq. (8) can be deduced (Bonamy et al. 2008):

$$K = \frac{\Gamma_0}{c_0} \quad V_m = \frac{V c_0}{2\Delta_0} \quad \Delta_0 = \left(\frac{3\Gamma_0 c_0^4}{E d^3}\right)^{1/2} \tag{12}$$

where V is the opening velocity of the displacement Δ_0 imposed between the two plates. It is worth mentioning at this point that visco-elastic effects may be important over the velocity range explored experimentally in Måløy et al. (2006). However, as we will see below, the simple linear elastic description proposed here succeed to capture *the scaling features* of the dynamics statistics. Equation (8) was solved numerically using a fourth-order Runge-Kutta scheme, for a front $f(z,t)$ propagating within a 1024×1024 uncorrelated map $\eta(z,x)$ with zero average and unit variance, with various values for the parameters μ, k, c_0, v_m. To characterize the local dynamics of the resulting crack front, we adopted the analysis procedure proposed by Måløy et al. (2006) and computed at each point (z,x) of the recorded region the time $w(z,x)$ spent by the crack front within a small 1×1 pixel^2 region as it passes through this position. A typical gray-scale image of this so-called waiting time map is presented in the upper panel of Fig. 4b. The intermittency reflects in the numerous and various regions of gray level. It looks

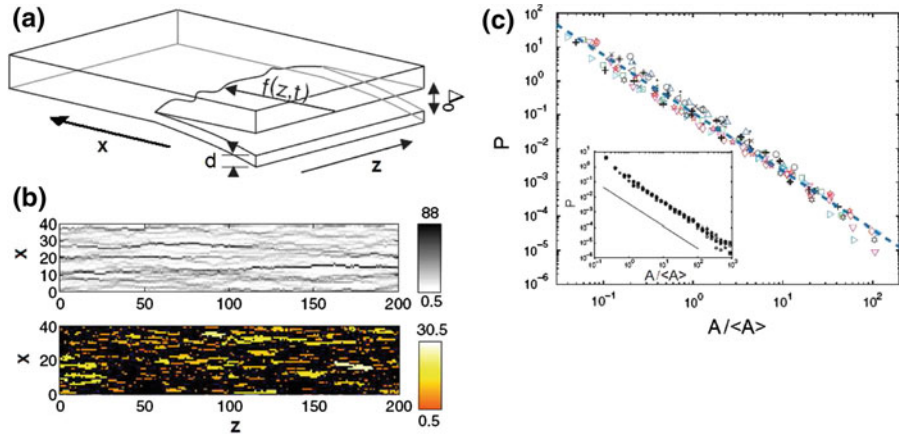

Fig. 4 Effect of material heterogeneities on the local dynamics of a crack: **a** Sketch of the fracture test **b** Definition of the avalanches from the spatio-temporal evolution of the crack front illustrated here for numerical simulations of Eq. (8) (see text for details). **c** Distribution of avalanche sizes measured during the intermittent propagation of a crack at the heterogeneous interface between two PMMA plates (courtesy of K.J. Måløy and S. Santucci, from Måløy et al. 2006). The power-law behavior with exponent $\tau_0 = 1.7$ is in agreement with the results of the simulations shown in *inset*

very similar to those observed experimentally in Måløy et al. (2006).

These waiting time maps are then binarized defining avalanches as clusters of connected pixels where $w(z, x)$ is smaller than a given threshold $C\langle w\rangle$, where $\langle\rangle$ denotes averaging over both time and space within the steady regime. A typical avalanches map is represented in the lower panel of Fig. 4b. In addition in this representation, the avalanche duration is given by the cluster color according to the color scale given in the inset. Each of these avalanches is characterized by several quantities: Their width L_z, their thickness L_x, their area A and their duration D. The local front dynamics can then be characterized by computing the distribution and the scaling between these various quantities. Figure 4c represents the area distribution in logarithmic representations as obtained from the numerical simulations in inset, and as measured experimentally in Måløy et al. (2006). At large scales, these quantities such as area and duration are found to be power-law distributed (Bonamy et al. 2008):

$$\begin{aligned} P(A) &\propto A^{-\tau_0} \quad \text{with} \quad \tau_0 \simeq -1.65 \\ P(D) &\propto D^{-\alpha_0} \quad \text{with} \quad \alpha_0 \simeq -2.1 \end{aligned} \tag{13}$$

In addition, power-law relationships are observed between L_x and L_z, and between D and A:

$$\begin{aligned} L_x &\propto L_z^H \quad \text{with} \quad H \simeq 0.65 \\ D &\propto L^{\gamma_0} \quad \text{with} \quad \gamma_0 \simeq 0.4 \end{aligned} \tag{14}$$

All these scaling and distributions are found to be independent of the precise values of the equation parameters—provided that k and v_m remains small enough—and of the precise distribution of η—provided that it remains short-range correlated. Moreover, the area distribution and the scaling between L_z and L_x are found to be in very good agreement with experimental observations reported in Måløy et al. (2006).

The stochastic LEFM description of crack growth proposed in Eq. (8) succeeds to reproduce the intermittency statistics observed experimentally on the interfacial crack growth along the weak heterogeneous interface within PMMA blocks. And this intermittency statistics is likely to be universal: As mentioned before, the equation of motion (Eq. 8) suggests that the onset of crack growth is analogue to a critical transition between a stable phase, where the crack remains pinned by the material heterogeneities and a moving phase, where the mechanical energy available at the crack tip is sufficient to make the front propagate (Schmittbuhl et al. 1995). While growing, the crack decreases its mechanical energy and gets pinned again. Provided that the growth is slow enough, this retro-action process keeps the system close to the critical point during the whole propagation, as for self-organized-critical systems (Bonamy et al. 2008). As such, the statistics of the front dynamics are expected to be universal, independent of the microscopic and macroscopic details of

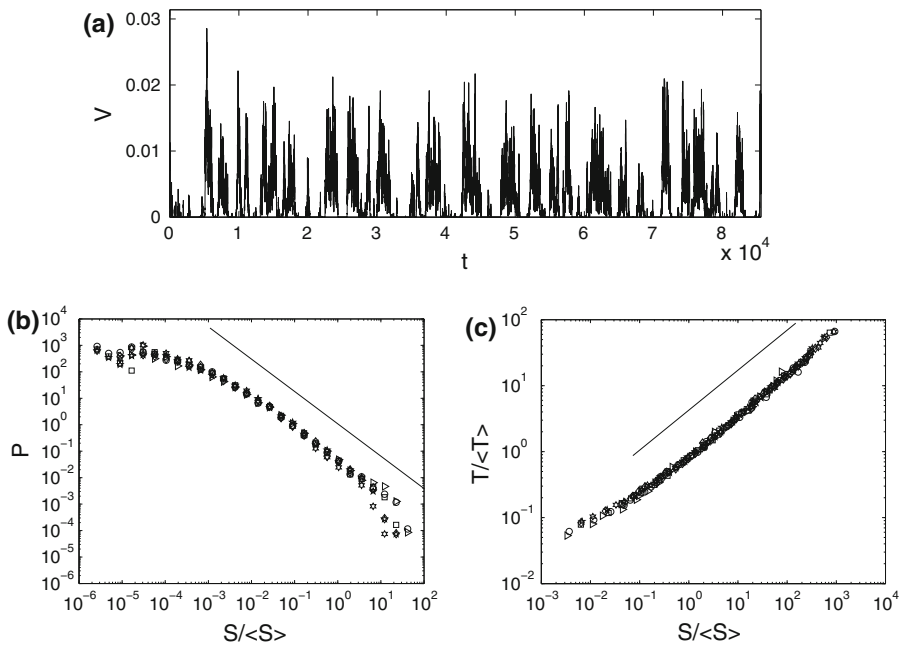

Fig. 5 Effect of material heterogeneities on the global dynamic of a crack: **a** Typical time evolution of the spatially averaged instantaneous crack velocity as predicted from Eq. 8. The parameters are set to $\mu = 1, G_0(c_0, 0) = 1, \delta\Gamma = 1, c_0 = 0, k = 10^{-3}$ and $v_m = 10^{-2}$. **b** Distribution of normalized burst size $S/\langle S\rangle$. **c** Scaling between the normalized burst duration $T/\langle T\rangle$ and the normalized burst size $S/\langle S\rangle$. In both plots (**b**) and (**c**), the axes are logarithmic. The various symbols correspond to various values of v_m and k in Eq. 8. The *straight lines* correspond to $P(S/\langle S\rangle) \propto (S/\langle S\rangle)^{-\tau}$ and $T/\langle T\rangle \propto (S/\langle S\rangle)^{a}$ with $\tau = 1.28$, and $a = 0.55$

the system, namely of the material microstructure and of the loading conditions.

To some extent, the fluctuation statistics on crack dynamics can be predicted theoretically using tools issued from out-of-equilibrium statistical physics like Functional Renormalization Methods (FRG) or numerical simulations. In this respect, the global dynamics of the crack front, i.e. the fluctuations of the spatially averaged instantaneous velocity $\overline{v}(t) = \langle \partial f/\partial t\rangle_z$ can be determined theoretically. Typical time evolution of $\overline{v}(t)$ is represented in Fig. 5a. Intermittency reflects in the large bursts that can be evidenced in this signal. Avalanches are then defined as zones where $\overline{v}(t)$ is larger than a given threshold $v_c = C\langle v\rangle$ where $\langle v\rangle$ denotes the mean value of the crack velocity averaged over both time and space within the steady regime. The duration T and size S of a given burst are then computed as the interval between two successive intersections of $\overline{v}(t)$ with v_c, and the integral of $\overline{v}(t) - v_c$ between the same points, respectively. The distributions of S and T as well as the scaling between T and S predicted by Eq. (6) have been derived via FRG methods and numerical simulations in the context of domain wall motion in disordered ferromagnets Durin and Zapperi (2006):

$$\begin{aligned} P(S) &\propto S^{-\tau}\Phi_S(S/S_0) \quad \text{with } \tau \simeq 1.28 \\ P(T) &\propto T^{-\alpha}\Phi_T(T/T_0) \quad \text{with } \alpha \simeq 1.50 \\ T &\propto S^{a} \quad \text{with } a \simeq 0.55 \end{aligned} \tag{15}$$

where $\Phi_S(x)$ and $\Phi_T(x)$ are functions constant for $x \ll 1$ and decaying rapidly with x for $x \gg 1$. These distributions depend neither on the precise values of k, v_m and C-provided that k and v_m are small enough, nor on the random term η-provided that it remains short-range correlated. It coincides well with the distribution measured from the numerical solution of Eq. (8) plotted in Fig. 5b,c. On the other hand, the upper cut-offs S_0 and T_0 are predicted to depend on the compliance k as:

$$\begin{aligned} S_0 &\propto k^{-1/\sigma} \quad \text{with } \sigma \simeq 1.44 \\ T_0 &\propto k^{-1/\Delta} \quad \text{with } \Delta \simeq 1.30 \end{aligned} \tag{16}$$

4 Discussion

The theoretical framework presented here and the comparison with experimental results obtained on heterogeneous materials open new perspectives for the prediction of macroscopic quantities of direct interest for Engineering and Applied Science. Indeed, it relates microstructural properties of a brittle material with its effective fracture energy or the crack velocity.

At first, it defines the effective fracture energy of an inhomogeneous brittle solid as the depinning driving force necessary to make the crack propagate within the material. This suggests a simple way to proceed to its homogenization, and average the local values of the fracture energy (Roux and Hild 2008). We can use an estimate of the force at depinning as proposed e.g. in Barabási and Stanley (1995) to compute the effective fracture energy

$$G_c \simeq \Gamma_0 + \pi(\delta\Gamma)^2/\Gamma_0. \tag{17}$$

It is important to note that the fracture energy of inhomogeneous solids can be significantly larger than their homogeneous conterpart, even though they have both the same average fracture energy $\Gamma_0 = \langle G_c(x, y, z)\rangle_{x,y,z}$. This results in a significant toughening induced by randomly distributed heterogeneities in a brittle material, analogous to the toughening effect shown in the context of periodic heterogeneous media by Gao and Rice (1989) and Xu et al. (1998).

The disorder induced toughening effect opens new perspectives in the field of Material Science and Engineering: microstructure of brittle solids can be tuned and controlled to increase significantly their level of heterogeneity, and so their resistance to failure, as well as their lifetime. For example, this effect is relevant when dealing with brittle glass ceramics, the fracture energy of which increases while increasing either their porosity (Coronel et al. 1990), or the volumic fraction of a secondary phase in the solid (Hing and McMillan 1973). This is a simple way to enhance the resistance of brittle solids while keeping their highly brittle behavior.

Beyond the disorder induced toughening effect, the universality manifested around the depinning onset allows to determine the distribution of effective macroscopic fracture energy in heterogeneous materials of finite size (Roux et al 2003; Charles et al. 2004; Vandembroucq et al. 2004). This distribution is found (1) to depend only on the mean value Γ_0 and standard deviation $\delta\Gamma$ of the local fracture energy, (2) to exhibit a universal scaling between its second moment and the specimen size and (3) to take a universal toughness distribution for large enough specimens. The effect of temperature has also been discussed in Vandembroucq et al. (2004).

Finally, we would like to discuss the implications of our model described by Eq. (8) on the morphology of the crack. As underlined in Sec. 2, this equation can be linearized as far as the crack perturbations remain sufficiently small compared to the typical size ξ of heterogeneities in the solid so that the noise term $\eta(z, f(z,t))$ can be approximated by $\eta(z, \overline{f}(t))$. Non-linearity becomes relevant when $|\delta f| \gg \xi$, leading to the pinning of the front at small driving forces. This effect can be evidenced on the geometry of the crack front:

(i) In the linear regime, the crack front is self-affine, i.e. the correlation function $\Delta f(\delta z, t) = \langle[f(z+\delta z, t) - f(z,t)]^2\rangle_z^{1/2}$ of its in-plane perturbations evolve as $\Delta f \sim \delta z^{\zeta_l}$ where the so-called roughness exponent $\zeta_l = 0.5$ can be calculated by Fourier transform of Eq. (8) as done in Pindra et al. (2008), in the context of brittle interfacial crack propagation [6] and in Tanguy and Vettorel (2004), in the context of the motion of a contact line on a disordered substrate.

(ii) In the non-linear regime, the geometry of the crack front is also self-affine, but the roughness exponent cannot be calculated exactly. Techniques such as renormalization (Ertas and Kardar 1994; Chauve et al. 2001) and numerical simulations (Rosso and Krauth 2002) provides however an approximated value $\zeta_p \simeq 0.39$.

As a result, Eq. (8) predicts that the in-plane perturbations of the crack front are characterized by two different scaling regimes, with roughness exponents $\zeta_l = 0.5$ at small scales ($\Delta f \ll \xi$), and $\zeta_p \simeq 0.39$ at larger scales. This second regime extends up to a cut-off length-scale L that scales with the compliance k as $L \propto k^{-\nu_k}$ with $\nu_k = 1/2$ (Bonamy 2009). For scale larger than L, the crack front is expected to exhibit logarithmic correlations. These predictions can be compared with recent experimental results obtained by direct observation of an interfacial crack propagating

[6] In Pindra et al. (2008), the authors compute the power spectrum of the perturbations $\Im \sim \frac{1}{q^2} \sim \frac{1}{q^{1+2\zeta_l}}$, leading to the value $\zeta_l = 0.5$ of the roughness exponent (see e.g. Feder 1988).

within two transparent plexiglass plates (Santucci et al. 2009) where disorder is introduced artificially by sand-blasting the plates surface with glass beads of different diameters d, corresponding roughly to the typical size ξ of heterogeneities at the weak interface: they observe two self-affine regimes with exponents $\zeta \simeq 0.57$ and $\zeta \simeq 0.35$ at small and large scale, respectively, with a transition observed close to $\Delta f \simeq d/5$. Despite the correct agreement with the theoretical predictions, note that the small scale regime is characterized by a multi-affine behavior not captured by Eq. (8). This might be either related to correlations between the values of fracture energy at scales comparable to the heterogeneity size, not assumed in this analysis, or due to large value of the local slope of the front, so that Eq. (2) is not valid anymore .

5 Conclusion

The propagation of a crack in brittle materials with weakly heterogeneous local properties has been investigated in the quasi-static limit. We extend the "standard" Linear Elastic Fracture Mechanics (LEFM) developed for homogeneous materials to the case of heterogeneous media by considering a random field of fracture energy. In our model, the motion of a crack is analogous to the one of an elastic line driven in a random medium and critical failure occurs when the external force is sufficiently large to depin the crack front from the heterogeneities of the material. In addition, we show that the compliance of the material results in an effective restoring force on the crack front that maintains it close to its equilibrium position provided by the balance of the external elastic energy release rate with the average fracture energy of the solid. Our description results in predictions on the dynamics of the crack that are compared with recent experimental results (Ponson 2009; Måløy et al. 2006). We show that the main features of *both* average dynamic and its fluctuations can be reproduced quantitatively by the proposed stochastic extension of Fracture Mechanics to inhomogeneous media. These results have important implications in Material Science and Engineering by providing a quantitative description of the toughening of brittle material induced by its heterogeneities. We hope that this link between the microstructural properties of brittle materials and their fracture energy or the crack velocity will help to design stronger materials with increased lifetime.

Acknowledgments The authors would like to thank G. Cordeiro and A. Bindal for their help in the experiments and J.-B. Leblond, S. Santucci and R. Toledo for helpful discussions. L. P. is supported by the European Union through a Marie Curie fellowship (PhyCracks project).

References

Adda-Bedia M, Katzav E, Vandembroucq D (2006) Second-order variation in elastic fields of a tensile planar crack with a curved front. Phys Rev E 71:066127

Atkinson BK (1984) Subcritical crack growth in geological materials. J Geophys Res 89:4077–4114

Ball RC, Larralde H (1995) Three-dimensional stability analysis of planar straight cracks propagating quasistatically under type I loading. Int J Frac 71:365–377

Barabási AL, Stanley HE (1995) Fractal concepts in surface growth. Cambridge University Press, Cambridge

Bonamy D (2009) Intermittency and roughening in the failure of brittle heterogeneous materials. J Phys D 42:214014

Bonamy D, Ponson L, Prades S, Bouchaud E, Guillot C (2006) Scaling exponents for fracture surfaces in homogeneous glass and glassy ceramics. Phys Rev Lett 97:135504

Bonamy D, Santucci S, Ponson L (2008) Crackling dynamics in material failure as the signature of a self-organized dynamic phase transition. Phys Rev Lett 101:045501

Bower AF, Ortiz M (1991) A 3-dimensional analysis of crack trapping and bridging by tough particle. J Mech Phys Solids 39:815

Charles RJ (1959) Static fatigue of glass II. J Appl Phys 29:1554–1560

Charles Y, Hild DVF, Roux S (2004) Material-independant crack arrest statistics. J Mech Phys Solids 52:1651–1669

Chauve P, Doussal PL, Wiese KJ (2001) Renormalization of pinned elastic systems: how does it work beyond one loop? Phys Rev Lett 86:1785

Coronel L, Jernot JP, Osterstock F (1990) Microstructure and mechanical properties of sintered glass. J Mat Sci 25:4866–4872

Daguier P, Nghiem B, Bouchaud E, Creuzet F (1997) Pinning and depinning of crack fronts in heterogeneous materials. Phys Rev Lett 78:1062–1065

Doussal PL, Wiese KJ, Chauve P (2004) Functional renormalization group and the field theory of disordered elastic systems. Phys Rev E 68:026112

Duemmer O, Krauth W (2007) Depinning exponents of the driven long-range elastic string. J Stat Mech 1: 01019

Durin G, Zapperi S (2006) The Barkhausen effect. In: Bertotti G, Mayergoyz I (eds) The science of hysteresis. Academic Press, Amsterdam pp 181–267

Ertas D, Kardar M (1994) Critical dynamics of contact line depinning. Phys Rev E 49:R2532

Feder J (1988) Fractals. Plenum, New York

Feigelman MV, Geshkenbein VB, Larkin AI, Vinokur VM (1989) Theory of collective flux creep. Phys Rev Lett 63:2303–2306

Freund LB (1990) Dynamic fracture mechanics. Cambridge University Press, Cambridge

Gao H, Rice JR (1989) A first-order perturbation analysis of crack trapping by arrays of obstacles. J Appl Mech 56:828–836

Hing P, McMillan PW (1973) The strength and fracture properties of glass-ceramics. J Mat Sci 8:1041–1048

Koivisto J, Rosti J, Alava MJ (2007) Creep of a fracture line in paper peeling. Phys Rev Lett 99:145504

Kolton AB, Rosso A, Giamarchi T (2005) Creep motion of an elastic string in a random potential. Phys Rev Lett 94:047002

Måløy KJ, Santucci S, Schmittbuhl J, Toussaint R (2006) Local waiting time fluctuations along a randomly pinned crack front. Phys Rev Lett 96:045501

Movchan AB, Gao H, Willis JR (1998) On perturbations of plane cracks. Int J Solids Struct 35:3419–3453

Nara Y, Kaneko K (2005) Study of subcritical crack growth in andesite using the double torsion test. Int J Rock Mech Min Sci 42:521–530

Obreimoff JW (1930) The splitting strengh of mica. Proc Roy Soc Lond A 127:290

Pindra N, Lazarus V, Leblond JB (2008) The deformation of the front of a 3D interface crack propagating quasistatically in a medium with random fracture properties. J Mech Phys Solids 56:1269–1295

Ponson L (2007) Crack propagation in disordered materials: how to decipher fracture surfaces. Ann Phys 32:1–128

Ponson L (2009) Depinning transition in the failure of inhomogeneous brittle materials. Phys Rev Lett 103:055501

Ponson L, Bonamy D, Bouchaud E, Cordeiro G, Toledo R, Fairbairn E (2007) Path and dynamics of a crack propagating in a disordered material under mode I loading. In: Carpinteri A et al. (eds) Proceeding FRAMCOS-6, pp 63–67

Ramanathan S, Ertas D, Fisher DS (1997) Quasistatic crack propagation in heterogeneous media. Phys Rev Lett 79:873–876

Rice JR (1985) First-order variation in elastic fields due to variation in location of a planar crack front. J Appl Mech 52:571–579

Rosso A, Krauth W (2002) Roughness at the depinning threshold for a long-range elastic string. Phys Rev E 65:025101(R)

Rosso A, Doussal PL, Wiese KJ (2007) Numerical calculation of the renormalization group fixed-point functions at the depinning transition. Phys Rev B 75:220201

Roux S, Hild F (2008) Self-consistent scheme for toughness homogenization. Int J Frac 166:154–159

Roux S, Vandembroucq D, Hild F (2003) Effective toughness of heterogeneous brittle materials. Eur J Mech A/Solids 22:743–749

Santucci S, Grob M, Toussaint R, Schmittbuhl J, Hansen A, Måløy KJ (2009) The complex morphology of interfacial crack fronts. Private communication

Santucci S, Vanel L, Ciliberto S (2004) Subcritical statistics in rupture of fibrous materials: experiments and models. Phys Rev Lett 93:095505

Schmittbuhl J, Roux S, Vilotte JP, Måløy KJ (1995) Interfacial crack pinning: effect of nonlocal interactions. Phys Rev Lett 74:1787–1790

Tanguy A, Vettorel T (2004) From weak to strong pinning I: a finite size study. Eur Phys J B 38:71–82

Vandembroucq D, Skoe R, Roux S (2004) Universal depinning force fluctuations of an elastic line: application to finite temperature behavior. Phys Rev E 70:051101

Wiederhorn SM (1967) Influence of water vapor on crack propagation in soda-lime glass. J Am Ceram Soc 50:407–414

Wiederhorn SM, Johnson H, Dinessand AM, Heuer AH (1974) Fracture of glass in vacuum. J Am Ceram Soc 57

Xu G, Bower A, Ortiz M (1998) The influence of crack trapping on the toughness of fiber reimforced composites. J Mech Phys Sol 46:1815